Hard X Ray Holographic Diffraction Imaging

Lorenz-M. Stadler,[1,*] Christian Gutt,[1] Tina Autenrieth,[1] Olaf Leupold,[1] Stefan Rehbein,[2] Yuriy Chushkin,[3] and Gerhard Grübel[1]

[1]*HASYLAB at DESY, Notkestr. 85, 22607 Hamburg, Germany*
[2]*BESSY GmbH, Albert-Einstein-Str. 15, 12489 Berlin, Germany*
[3]*ESRF, BP220, 38043 Grenoble Cedex, France*

(Received 15 February 2008; published 20 June 2008)

We determine the absolute electron density of a lithographically grown nanostructure with 25 nm resolution by combining hard x-ray Fourier transform holography with iterative phase retrieval methods. While holography immediately reveals an unambiguous image of the object, we deploy in addition iterative phase retrieval algorithms for pushing the resolution close to the diffraction limit. The use of hard (8 keV) x rays eliminates practically all constraints on sample environment and enables a destruction-free investigation of relatively thick or buried samples, making holographic diffraction imaging a very attractive tool for materials science. We note that the technique is ideally suited for subpicosecond imaging that will become possible with the emerging hard x-ray free-electron lasers.

DOI: 10.1103/PhysRevLett.100.245503 PACS numbers: 61.05.C−, 42.30.Rx, 68.37.Yz

Nanoscience mandates the ability to characterize the structure of objects on the nanoscale. Among the most commonly used techniques for that purpose are scanning-electron (SEM) and atomic-force microscopy (AFM), although their applicability is generally limited to surface structures. Transmission electron microscopy (TEM) can look into a material, but delicate nanostructures are likely to be disturbed or destroyed by the tedious thinning procedures accompanying TEM sample preparation. In addition, all these methods are quasistatic; i.e., their potential to trace dynamic processes is very limited. Hard x rays, on the other hand, can overcome all the above limitations. A wavelength in the order of $\lambda \approx 1$ Å allows for excellent spatial resolution, and the high penetration into matter permits to study thick samples or even buried structures in an easy-to-realize experimental setup. But most importantly, hard x-ray free-electron lasers [1,2] will push the achievable time resolution many decades down to the femtosecond (fs) regime. Here, we demonstrate how coherent hard x rays can be used for a determination of the absolute electron density of a lithographically tailored gold nanostructure (the letter P) from a single diffraction experiment, yielding both the shape and the height of the sample. We combine Fourier transform holography, which—by a single Fourier transform—gives an unambiguous image of the sample structure, with iterative phase retrieval procedures that enable us to achieve a spatial resolution almost reaching the diffraction limit.

In this lensless imaging process a coherent diffraction pattern of the object needs to be inverted by computational means. Since only the absolute square of the diffraction amplitudes, the diffraction intensities, can be measured, the information on the phase of the scattered photons is lost. The phase information is however needed for computationally inverting the diffraction pattern. One way to overcome this problem is to encode the phase in the interference of the scattered photons with a reference wave, producing a hologram at the detector. Attempts to use holographic techniques with hard x rays have however been rather limited up to now and experiments relied either on crystals as objects [3] or on waveguides for creating a reference beam [4]. In FTH [5–8] phase retrieval becomes particularly simple, since in a typical setup the object and a spatially nearby reference are coherently illuminated and a single Fourier transform of the recorded hologram yields the convolution of the object and reference amplitudes. The spatial resolution achievable with FTH is comparable to the reference source size [9,10].

Provided the sampling of the diffraction pattern is sufficiently high [11], the FTH result can be used as starting point for further iterative phase retrieval in order to increase the resolution [12]. In the latter method, which is also known as coherent diffraction imaging (CDI), algorithms are used that cycle between real and Fourier space, applying appropriate constraints in each domain [13]. The minimum constraints are the approximate shape of the object, the so-called support, and the measured diffraction amplitudes. Essentially, the achievable spatial resolution is diffraction-limited, i.e., determined by the maximum photon momentum transfer. This compares very favorably to hard x-ray microscopes. Because of the difficulties in producing appropriate lenses, the achievable resolution is typically about 50–100 nm with today's zone plates [14] and compound refractive lenses, respectively, and it seems to be difficult to reach a resolution below 30 nm [15]. Examples for CDI experiments can be found in the literature, both for measurements with soft [16,17] and with hard x rays [18,19]. The main problem in CDI is to define the object support without having any additional information like an FTH result. In most cases, information on low spatial frequencies is not accessible due to an extended beam stop blocking the direct beam to prevent detector

damage, which has severe consequences for the convergence of the reconstruction algorithms and can be overcome by appropriate algorithms [20,21] only to a certain extent.

Here, we show for the first time results from hard x ray HDI—a combination of FTH and iterative phase retrieval methods in order to overcome the limitations of conventional CDI as mentioned above. We lithographically fabricated a nanoscale gold structure (the block letter P) on a 50 nm-thin Si_3N_4 membrane, with the letter elements about 200 nm in widths and approximately 220 nm in height. Five gold dots with about 175 nm diameter and 220 nm height were equally placed on a circle of radius $r = 2.5$ μm around the object, each acting as reference source in the scattering process. In this straightforward form of spatial multiplexing each source generates a unique image upon reconstruction. The multiple images can then be averaged in order to increase the image quality [10].

The experiment was carried out at beam line ID10C at the European Synchrotron Radiation Facility in Grenoble, France. A beam of partially coherent hard x-ray photons (energy $E = 8$ keV and wavelength $\lambda = 1.55$ Å, respectively) was used. Temporal coherence was ensured by a Si(111) channel-cut monochromator ($\Delta E/E \approx 10^{-4}$) and roller-blade slits were used to select a spatially coherent beam cross-section $A_0 = 10 \times 10$ μm^2 with an intensity of $I_0 \approx 1.4 \times 10^8$ photons per second. Two pairs of guard slits were used to clean the beam from parasitic slit scattering before illuminating the sample. The diffraction pattern was recorded in transmission geometry with a direct-illumination charge-coupled device (Princeton Instruments, 1242×1152 pixels, 22.5×22.5 μm^2 pixel size) at a distance of $L = 3.29$ m from the sample. For reducing air scattering we used an evacuated flight tube with kapton windows, whereas the sample as well as the slits were situated in air. A beam stop (1 mm diameter) at the end of the flight tube was used to block the direct beam and some remaining parasitic slit scattering at very small angles.

Figure 1(a) shows the recorded hologram in a 1094×1094 pixel-wide array, almost extending to the edges of the detector. The image is the sum of 200 single pictures, 3 s exposed each. A single Fourier transform of the measured intensities gives the spatial autocorrelation of the overall object, including the crosscorrelation between the object and the dots, which directly yields the object shape and its complex conjugate (a 180°-rotated copy) for each dot [10]. Since for each reference the object consists of the letter P plus the 4 other references, the reference sources are imaged as well. The central part of the inverted hologram is shown in Fig. 1(b). The letter P is clearly recognizable. Its shape is, however, slightly distorted and the contrast is reduced by a wavy background. This image degradation stems from the considerable number of bad pixels in the diffraction pattern, i.e., pixels that were either blocked by the beam stop or damaged or (in few cases, near the central beam stop) containing some remaining parasitic slit scattering. In addition, the relatively big reference-source size causes a slight blurring of the P structure in the FTH reconstruction, which is a small effect in our case.

In order to improve the statistics of the FTH result we average the 5 independent subimages. This average, shown as inset in the right upper corner of Fig. 1(b), still exhibits some small distortions and a nonconstant background, but features appear already quite clearly. Qualitatively, this result compares well to the scanning-electron micrograph depicted in the right lower corner of Fig. 1(b). The averaged FTH result is thus extremely well suited as starting point for further iterative phase retrieval algorithms that allow to push the spatial resolution down to the diffraction limit [16,17].

Additionally, we may also look at the FTH phases that are shown in Fig. 2. In general, x rays passing through a material of thickness z experience a phase shift $\Delta\phi$ according to $\Delta\phi = (2\pi/\lambda)\delta z$, where δ denotes the real part

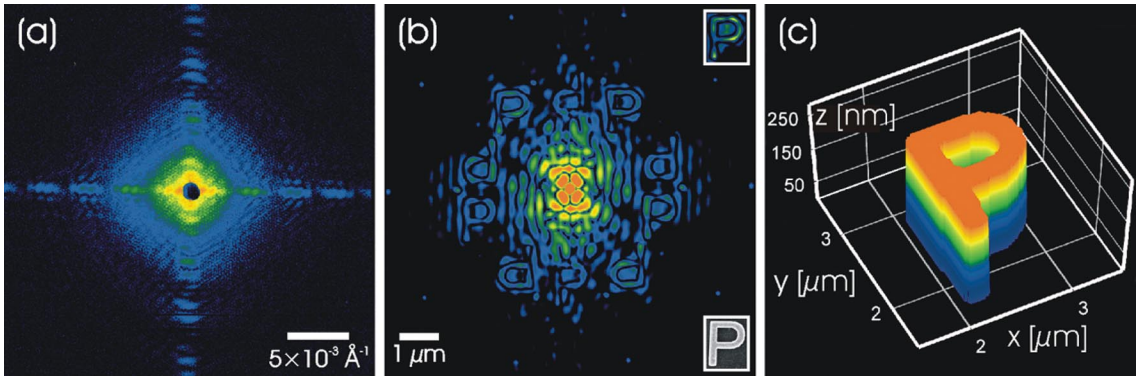

FIG. 1 (color). HDI processing of a single diffraction experiment. (a) Hologram of the lithographically grown gold nanostructure (block letter P), recorded with partially coherent 8 keV photons. Logarithmic pseudocolor scale. (b) Central part of the modulus of the Fourier transformed hologram, imaging the object and its rotated copy 5 times each. Logarithmic pseudocolor scale. The inset in the upper right corner shows the average of the 5 independent FTH results on a linear pseudocolor scale. For comparison, an SEM image is shown as inset in the right lower corner. (c) Visualization of the central object geometry as derived from the electron density profile.

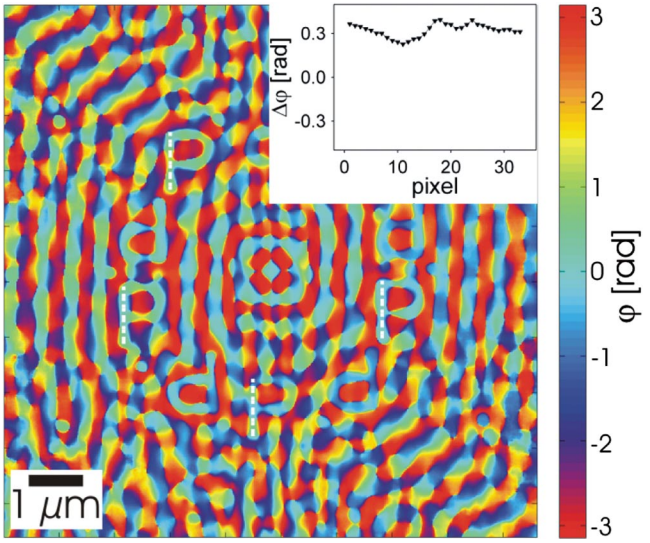

FIG. 2 (color). Central part of the phases of the Fourier transformed hologram. The object phases are affected by the phase structure which is caused by missing detector pixels. The inset shows the *average* of slices (indicated by the dashed white lines) within the 5 individual object image regions through the *difference* $\Delta\varphi$ between the experimental and simulated data, where a homogeneous sample height was assumed and missing detector pixels were accounted for.

of the material's refractive index at a specific photon energy. In the Fourier transform of the hologram we are sensitive to the *difference* between the x-ray phase shift in the reference and the sample structure. Provided sample and reference are illuminated with a plane wave, the phase in the FTH object image is $\varphi = 0$ at all points where the heights of object and reference dot are equal and $\varphi = (2\pi/\lambda)\delta\Delta z$ at points with a height difference of Δz. In Fig. 2 the object is well recognizable although φ is affected by a strong phase structure, which is caused by the missing pixels due to the beam stop and local detector damage. Since we know those pixels, we can account for them and derive quantitative information about the true object phases and the object height, respectively. Assuming a homogeneous sample height we simulate the corresponding FTH phases while accounting for the bad detector pixels as well as for the intensity in the measurement together with Poisson statistics [22]. To verify the quality of our assumption we take the difference between the experimental and simulated data, $\Delta\varphi$, and further average over the regions containing the 5 independent object images [22]. The inset in Fig. 2 shows a slice through that map, corresponding to the *average* of slices through $\Delta\varphi$ at positions indicated by the dashed white lines in the main panel. From that cut we obtain $\langle\Delta\varphi\rangle = 0.323 \pm 0.045$ rad. This difference is explained by a Fresnel phase $\tilde{\varphi}$ that forms between the object and the reference dots, since in the experiment the sample was situated $l \approx 0.48$ m downstream of the beam-defining slits; i.e., the sample was not illuminated by a plane wave but by the Fresnel diffraction of the slits. Following Ref. [23] we calculate the mean $\tilde{\varphi}$ for the object as

$$\tilde{\varphi} = \frac{1 + \Delta\lambda/\lambda}{2} r^2 \left(\frac{2\pi}{\lambda L} + \frac{2\pi}{\lambda l}\right), \quad (1)$$

yielding $\tilde{\varphi} \approx 0.3$ rad in excellent agreement with the above finding. The standard deviation of $\Delta\varphi$ corresponds to ≈ 23 nm—a quantitative measure of the homogeneity of the sample height.

For the iterative CDI procedures, we defined an initial support based on the *P* shape of the FTH average plus 5 circles at the reference-source positions. We then used the standard CDI algorithms of error reduction and hybrid-input output [13] and also allowed for further support refinement by the so-called shrink wrap method [21], which mainly affected the actual support of the reference dots. To be sure to have a clear result 100 independent phase retrieval runs (950 iterations each) were carried out.

Figure 3(a) shows the average amplitudes of those runs, yielding an object shape and support, respectively, in excellent agreement with the SEM finding. The small hot spot in the actual amplitude values, approximately in the middle of the long upright bar of the P letter, is an artifact due to the partial coherence of the x-ray beam [24]. The theoretical spatial resolution, corresponding to the maximum photon momentum transfer $\mathbf{Q}$, recorded at the edge of the Fourier transform array, was 20.7 nm. From line scans through an individual reconstruction result, illustrated in Fig. 3(b), we derive a resolution of ≈ 25 nm, which comes close to the theoretical value.

We note that the computing time for getting from the diffraction pattern [Fig. 1(a)] to the final object electron density as anticipated in Fig. 1(c) is very small. The computation time for the single Fourier transform of the measured hologram and the averaging of the 5 individual object images [Fig. 1(b)] is negligible. A successful phase

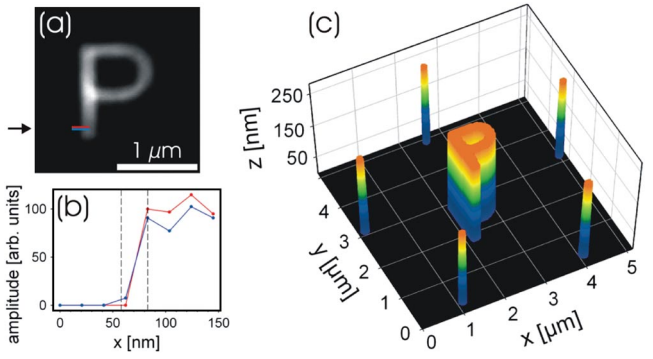

FIG. 3 (color). Results from the FTH-based phase retrieval runs. (a) Average amplitude of 100 phase retrieval runs. Linear gray scale. (b) Slices through an individual phase retrieval result at positions indicated by the red and blue line at the height of the eye-guiding arrow in (a), demonstrating a resolution of ≈ 25 nm (compare dashed lines). (c) Visualization of the object geometry (letter plus reference dots) as determined from the electron density profile.

retrieval run that makes use of the FTH results takes about 10 min on a standard PC.

The object electron density can be precisely derived via the relation

$$\frac{I_s}{(I_0/A_0)\Delta\Omega} = r_0^2\left[\int \langle\rho\rangle_z(x,y)e^{i(Q_x x+Q_y y)}dxdy\right]^2, \quad (2)$$

with I_s the detected scattering intensity in the solid angle $\Delta\Omega$, $r_0 = 2.82 \times 10^{-15}$ m the classical Thomson electron radius, and Q_x (Q_y) the x (y) component of the scattering vector $\mathbf{Q}$. $\langle\rho\rangle_z(x,y)$ denotes the electron number density projected along the z direction (parallel to the x-ray beam) and is defined as

$$\langle\rho\rangle_z(x,y) := \int \rho(x,y,z)dz. \quad (3)$$

From the phases of the inverted hologram we can assume that our sample has a homogeneous electron density (compare Fig. 2), and thus $\langle\rho\rangle_z(x,y)$ becomes a constant, identical to the number of gold electrons per unit volume (4653 nm^{-3}) multiplied by the mean sample height h. This implies that the integral on the right hand side of Eq. (2) comprises only the Fourier transform of the object support multiplied by a constant. Since we precisely know the support from our reconstruction result based on the FTH findings [compare Fig. 3(a)], we can compute the integral. Inspection of Eq. (2) yields $h = 235$ nm $\pm$ 10%, where the error is derived from the FTH phases, see above. The result is visualized in Fig. 3(c). Our finding is in very good agreement with an AFM measurement, confirming that the nanostructure has a homogeneous height with a mean of $h \approx 220$ nm.

In conclusion, we have shown that holographic diffraction imaging (HDI) with hard x rays is an excellent technique for determining electron density profiles on the nanoscale. By combining the FTH result with iterative phase retrieval methods we push the spatial resolution toward the diffraction limit. In a straightforward way one quickly arrives from a single diffraction measurement at the object electron density, as illustrated in Figs. 1(a)–1(c). By virtue of this concept we determined the absolute electron density and derived both shape and height of a lithographic gold nanostructure. The presented approach with coherent hard x rays is ideally suited for applications in materials science, where samples can be thick, may consist of buried structures, or have to be measured under extreme conditions such as high pressure. Finally, we envision experiments of similar type to be carried out at future hard x-ray free-electron laser sources [1,2], where diffraction patterns can be collected within a single shot at the time scale of $\approx$10 fs, opening fascinating possibilities for imaging fast dynamic processes.

We thank A. Frömsdorf for characterizing our sample with AFM, A. Schropp for providing a pair of slits, and I. Vartaniants for discussion.

*lorenz.stadler@desy.de

[1] M. Altarelli, R. Brinkmann, M. Chergui, W. Decking, B. Dobson, S. Düsterer, G. Grübel, W. Graeff, H. Graafsma, J. Hajdu *et al.*, DESY XFEL Technical Design Report Nos. 2006-097, 22607, Hamburg, Germany, 2006.

[2] *LCLS The First Experiments*, edited by G. K. Shenoy and J. Stöhr (Stanford Linear Accelerator Center, Stanford, University, Stanford, CA 94309, 2000).

[3] T. Gog, P. M. Len, G. Materlik, D. Bahr, C. S. Fadley, and C. Sanchez-Hanke, Phys. Rev. Lett. **76**, 3132 (1996).

[4] C. Fuhse, C. Ollinger, and T. Salditt, Phys. Rev. Lett. **97**, 254801 (2006).

[5] G. W. Stroke and D. G. Falconer, Phys. Lett. **13**, 306 (1964).

[6] G. W. Stroke, Appl. Phys. Lett. **6**, 201 (1965).

[7] J. T. Winthrop and C. R. Worthington, Phys. Lett. **15**, 124 (1965).

[8] I. McNulty, J. Kirz, C. Jacobsen, E. H. Anderson, M. R. Howells, and D. Kern, Science **256**, 1009 (1992).

[9] S. Eisebitt, J. Lüning, W. F. Schlotter, M. Lörgen, O. Hellwig, W. Eberhardt, and J. Stöhr, Nature (London) **432**, 885 (2004).

[10] W. F. Schlotter, R. Rick, K. Chen, A. Scherz, J. Stöhr, J. Lüning, S. Eisebitt, C. Günther, W. Eberhardt, and O. Hellwig *et al.*, Appl. Phys. Lett. **89**, 163112 (2006).

[11] J. Miao, P. Charalambous, J. Kirz, and D. Sayre, Nature (London) **400**, 342 (1999).

[12] S. Eisebitt, M. Lörgen, W. Eberhardt, J. Lüning, S. Andrews, and J. Stöhr, Appl. Phys. Lett. **84**, 3373 (2004).

[13] J. R. Fienup, Appl. Opt. **21**, 2758 (1982).

[14] URL http://xradia.com.

[15] B. Lengeler, C. G. Schroer, M. Kuhlmann, B. Brenner, T. F. Günzler, O. Kurapova, F. Zontone, A. Snigirev, and I. Snigireva, J. Phys. D **38**, A218 (2005).

[16] H. N. Chapman, A. Barty, S. Marchesini, A. Noy, S. P. Hau-Riege, C. Cui, M. R. Howells, R. Rosen, H. He, and J. C. H. Spence *et al.*, J. Opt. Soc. Am. A **23**, 1179 (2006).

[17] H. N. Chapman, A. Barty, M. J. Bogan, S. Boutet, M. Frank, S. P. Hau-Riege, S. Marchesini, B. W. Woods, S. Bajt, and W. H. Benner *et al.*, Nature Phys. **2**, 839 (2006).

[18] J. Miao, J. E. Amonette, Y. Nishino, T. Ishikawa, and K. O. Hodgson, Phys. Rev. B **68**, 012201 (2003).

[19] M. A. Pfeifer, G. J. Williams, I. A. Vartanyants, R. Harder, and I. K. Robinson, Nature (London) **442**, 63 (2006).

[20] Y. Nishino, J. Miao, and T. Ishikawa, Phys. Rev. B **68**, 220101(R) (2003).

[21] S. Marchesini, H. He, H. N. Chapman, S. P. Hau-Riege, A. Noy, M. R. Howells, U. Weierstall, and J. C. H. Spence, Phys. Rev. B **68**, 140101(R) (2003).

[22] See EPAPS Document No. E-PRLTAO-101-058852 for the full map of the simulated φ and $\Delta\varphi$ averaged over the regions containing the 5 independent object images. For more information on EPAPS, see http://www.aip.org/pubservs/epaps.html.

[23] S. K. Sinha, M. Tolan, and A. Gibaud, Phys. Rev. B **57**, 2740 (1998).

[24] I. A. Vartanyants and I. K. Robinson, J. Phys. Condens. Matter **13**, 10593 (2001).